ISSN 1674-1056
http://cpb.iphy.ac.cn
http://iopscience.iop.org/cpb
中国物理 B
Chinese Physics
中国物理
Chinese Physics B

Bidirectional asymmetric acoustic focusing by two flat acoustic metasurfaces

Di-Chao Chen(陈帝超), Xing-Feng Zhu(朱兴凤), Qi Wei(魏琦), Da-Jian Wu(吴大建)

Citation: Chin. Phys. B . 2018, 27(12): 124302. **doi:** 10.1088/1674-1056/27/12/124302
Journal homepage: http://cpb.iphy.ac.cn; http://iopscience.iop.org/cpb

What follows is a list of articles you may be interested in

Thermoacoustic-reflected focusing lens based on acoustic Bessel-like beam with phase manipulation

An-Ru Hou(侯安茹), Wen-Ting Gao(高文婷), Jiao Qian(钱姣), Hong-Xiang Sun(孙宏祥), Yong Ge(葛勇), Shou-Qi Yuan(袁寿其), Qiao-Rui Si(司乔瑞), Xiao-Jun Liu(刘晓峻)

Chin. Phys. B . 2018, 27(12): 124301. **doi:** 10.1088/1674-1056/27/12/124301

Influence of mode conversions in the skull on transcranial focused ultrasound and temperature fields utilizing the wave field separation method: A numerical study

Xiang-Da Wang(王祥达), Wei-Jun Lin(林伟军), Chang Su(苏畅), Xiu-Ming Wang(王秀明)

Chin. Phys. B . 2018, 27(2): 024302. **doi:** 10.1088/1674-1056/27/2/024302

Broadband acoustic focusing by symmetric Airy beams with phased arrays comprised of different numbers of cavity structures

Jiao Qian(钱姣), Bo-Yang Liu(刘博阳), Hong-Xiang Sun(孙宏祥), Shou-Qi Yuan(袁寿其), Xiao-Zhu Yu(俞笑竹)

Chin. Phys. B . 2017, 26(11): 114304. **doi:** 10.1088/1674-1056/26/11/114304

Theoretical analysis of interaction between a particle and an oscillating bubble driven by ultrasound waves in liquid

Yao-Rong Wu(武耀蓉), Cheng-Hui Wang(王成会)

Chin. Phys. B . 2017, 26(11): 114303. **doi:** 10.1088/1674-1056/26/11/114303

Wideband dispersion removal and mode separation of Lamb waves based on two-component laser interferometer measurement

Yan-Feng Xu(徐琰锋), Wen-Xiang Hu(胡文祥)

Chin. Phys. B . 2017, 26(9): 094301. **doi:** 10.1088/1674-1056/26/9/094301

SPECIAL TOPIC — 60th Anniversary of the Department of Physics at the Nanjing Normal University

Bidirectional asymmetric acoustic focusing with two flat acoustic metasurfaces*

Di-Chao Chen(陈帝超), Xing-Feng Zhu(朱兴凤)†, Qi Wei(魏琦), and Da-Jian Wu(吴大建)‡

Jiangsu Key Laboratory on Opto-Electronic Technology, School of Physics and Technology, Nanjing Normal University, Nanjing 210023, *China*

(Received 15 August 2018; revised manuscript received 11 September 2018; published online 10 November 2018)

We design an asymmetric transmission system (ATS) with two flat acoustic metasurfaces (AMs) to yield bidirectional asymmetric acoustic focusing (BAAF). The acoustic waves could be focused on both sides of the ATS with different focal lengths and intensities. To achieve high intensity energy concentration, the accelerating acoustic beams are selected to realize the BAAF. The working bandwidth of the BAAF based on our ATS could reach ~ 0.4 kHz. It is found that by adjusting the distance between two flat AMs, the focal length and intensity of the bidirectional focusing could easily be modulated. Because the distance between two flat AMs is large enough, the BAAF even could be converted into a unidirectional acoustic focusing. The proposed BAAF may find applications in non-destructive evaluation, biomedical imaging and medical diagnosis.

Keywords: asymmetric focusing, acoustic metasurface, phase manipulation

PACS: 43.35.+d, 43.25.+y, 43.38.+n **DOI:** 10.1088/1674-1056/27/12/124302

1. Introduction

Acoustic metasurfaces (AMs) have received significant attention in recent years due to their compact planar subwavelength structures and unprecedented wave modulation capabilities.[1–8] Various applications have been achieved based on AMs including planar focusing,[9,10] acoustic imaging,[11] beam steering,[12,13] noise control,[14] and so on. Up to now, most of AMs yield symmetric manipulations for the acoustic waves coming from two opposite directions. More recently, several groups focused on the acoustic asymmetric transmission system (ATS).[15–18] For example, Jiang *et al.*[17] demonstrated an acoustic one-way AM which could realize three distinct unidirectional phenomena; *i.e.*, anomalous refraction, wave splitting and conversion of propagation wave to surface wave. A bilayer acoustic gradient metasurface was proposed to realize the controllable asymmetric transmission.[18]

Acoustic focusing is an important wave phenomenon and it has extensive applications in ultrasound imaging, biomedical therapy, particle trapping and manipulation.[19–23] AMs-enabled planar acoustic lens overcomes the geometrical and wave aberrations of the conventional acoustic focusing lenses.[24–26] In general, an AM lens is a symmetric system and the focal length and intensity of the focus are fixed. Recently, Xia *et al.*[27] designed a dual-layer metasurface to realize unidirection focusing. However, the bidirectional asymmetric acoustic focusing (BAAF) with different focal lengths and intensities is still unexplored.

In this paper, we design an ATS with two different flat AMs to realize the bidirectional asymmetric acoustic focusing. To achieve high intensity energy concentration, the accelerating acoustic beams with non-diffracting property are selected to realize BAAF. The acoustic field distributions of the BAAF are demonstrated numerically by using the finite element method (FEM). It is demonstrated that the acoustic waves could be focused on both sides of the ATS with different focal lengths and intensities. We further carefully study the influence of the space L between two AMs on the BAAF.

2. Bidirectional asymmetric acoustic focusing model

Figure 1 shows schematic diagrams of the ATS for BAAF. The ATS consists of two different flat AMs (AM-1 and AM-2) with a space L in between. The accelerating acoustic non-diffracting beams[28,29] are selected to realize the BAAF. When the acoustic plane wave normally impinges on the AM-1 on the left, the transmitted waves propagate along two parabolic trajectories: $y = ax^2$ $(y \leq 0)$ and $y = -ax^2$ $(y \geq 0)$ [marked as PT-1]. When acoustic wave normally impinges on the AM-2 on the right, the transmitted waves propagate along other two parabolic trajectories: $y = -bx^{1/2}$ $(y \leq 0)$ and $y = bx^{1/2}$ $(y \geq 0)$ [marked as PT-2]. Here, we define the propa-

*Project supported by the National Natural Science Foundation of China (Grant Nos. 11704193, 11674175, and 11704192), the "333" Project of Jiangsu Province, China (Grant No. BRA2017451), and the Postgraduate Research & Practice Innovation Program of Jiangsu Province, China (Grant No. KYCX18_1185).

†Corresponding author. E-mail: zhuxingfeng@njnu.edu.cn

‡Corresponding author. E-mail: wudajian@njnu.edu.cn

© 2018 Chinese Physical Society and IOP Publishing Ltd

gation directions of the waves normally incident on the AM-1 and AM-2 as the positive direction (PD) and negative direction (ND), respectively. For the PD case shown in Fig. 1(a), the transmitted waves through AM-1 are divided into PT-1, which further propagate through AM-2. Finally, the transmitted waves through the AM-2 are focused with a short focal length. In contrast, for the ND case shown in Fig. 1(b), the transmitted waves through AM-2 are divided into PT-2, which further transmit through AM-1 and hence focusing with a long focal length is achieved.

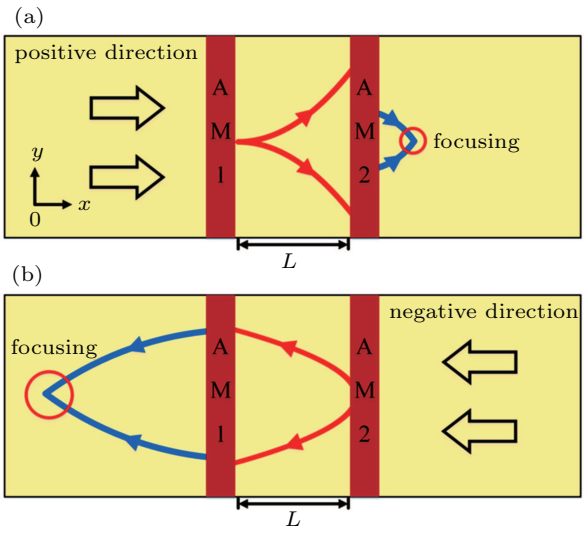


Fig. 1. (color online) Schematic diagram of the working principle of the asymmetric transmission system (ATS) for (a) positive direction (PD) case and (b) negative direction (ND) case.

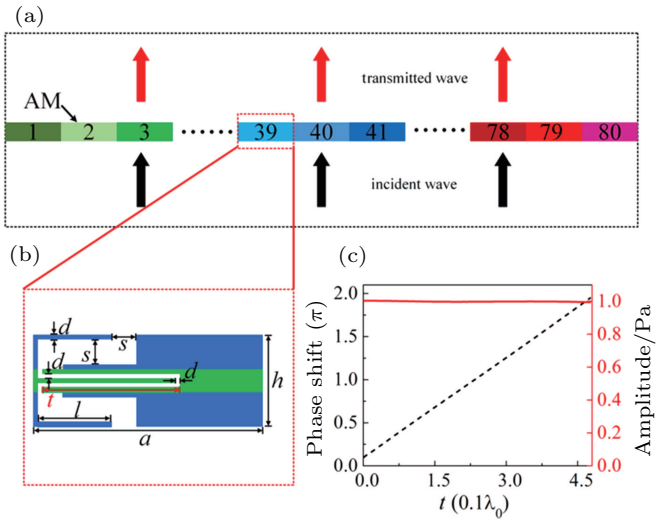


Fig. 2. (color online) (a) Arrangement of AM with 80 subunits. (b) Schematics of three-layered acoustic space-coiling (TAS) subunit. (c) Transmitted phase shifts (dashed line for left-hand scale) and amplitudes (solid line for right-hand scale) of TAS subunit as a function of t.

Next, we demonstrate a practical implementation of the proposed AM in air. Each AM is composed of 80 subunits with different phase shifts, as shown in Fig. 2(a). A three-layer acoustic space-coiling (TAS) structure is used as the subunit to build the AM.[30] Figure 2(b) shows the structure of a TAS subunit. Only on parameter t is picked to adjust the phase shift and amplitude through the TAS. The other parameters are set to be $s = 0.065\lambda_0$, $d = 0.01\lambda_0$, $l = 0.1538\lambda_0$, $a = 0.5\lambda_0$, and $h = 0.22\lambda_0$. Some other structural parameters, just like d and s, can also modulate the phase shift of the subunit, but the phase shift and amplitude cannot meet the requirement simultaneously. We calculate the distributions of the acoustic fields based on FEM (the commercial software COMSOL Multiphysics 5.2a). In the simulations, all microstructures with actual geometric sizes are fully considered. The plastic frame of the TAS is modeled as an acoustically rigid frame. The relative weights for varied diffractive branches are extracted after the scattering matrix of the complex sample have been calculated accurately. Air with mass density $\rho_a = 1.21$ kg/m^3 and acoustic speed $c_a = 343.2$ m/s is assumed to be the background medium and steel with mass density $\rho_s = 7800$ kg/m^3 and acoustic speed $c_s = 6,100$ m/s is selected as the medium of the acoustic metasurface. Figure 1(c) shows the transmitted phase shifts (the dashed line for left-hand scale) and amplitudes (the solid line for right-hand scale) of the acoustic plane wave through the TAS subunits as a function of t. The amplitude of the incident plane wave herein is fixed at 1 Pa and the working frequency is fixed at 3.432 kHz ($\lambda_0 = 10$ cm). It is observed with increasing t-value that the phase shift changes almost linearly from 0 to 2π while the transmission amplitude keeps a very high value.

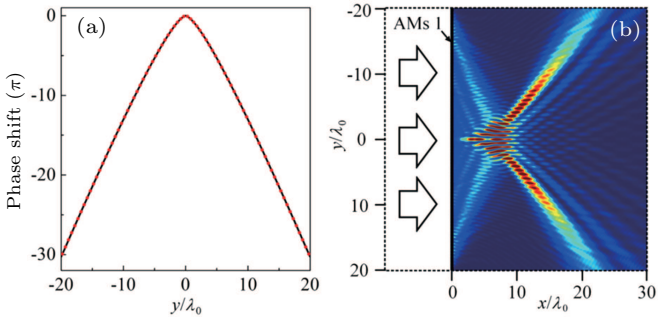


Fig. 3. (color online) (a) Spatial phase profile in y axis for two parabolic trajectories [$y = 0.5x^2$ ($y \le 0$) and $y = -0.5x^2$ ($y \ge 0$)] (PT-1) and (b) acoustic field distribution of the PT-1 through the AM-1. Scattered dots in panel (a) represent discrete phases of 80 subunits (one dot corresponds to one subunit).

For the AM-1, it is now required to derive the initial phase $\phi(x)$ corresponding to two parabolic trajectories $y = 0.5x^2$ ($y \le 0$) and $y = -0.5x^2$ ($y \ge 0$). The derivation is based on the caustic theory and geometrical properties where the parabolic trajectory can be constructed by multiple geometrical rays which are tangent to the curve itself.[28,29,31] In our case, the transverse modulation of the phase generates these geometrical rays at angles $\theta(y)$ with respect to the x axis, where $\mathrm{d}\phi(y)/\mathrm{d}y = k \cdot \sin[\theta(y)]$. This sets the relation between the angle $\theta(y)$ and the parabolic trajectory to be the following expression

$$\mathrm{d}\phi(y)/\mathrm{d}y = -k\sin(\theta) = kf'(x)/\sqrt{1+[f'(x)]^2}.$$

Therefore, the spatial phase profile on the y axis should be satisfied and is given as follows:

$$\phi(y) = k\left[\frac{1}{2}\ln(2\sqrt{0.5|y|}+\sqrt{1+2|y|}) - \sqrt{0.5y(1+2|y|)}\right]. \quad (1)$$

The solid line in Fig. 3(a) shows the spatial phase profile in the y axis based on Eq. (1). It is observed that two mirror-imaged phase profiles appear on two sides of y axis. According to this spatial phase profile, we design 80 TAS subunits with different t-values, and each subunit could provide the required transmitted phase shift [scattered dots in Fig. 3(a)] and ensure high transmitted amplitude. Because an acoustic plane wave normally impinges on the AM-1 from negative x axis, PT-1 acoustic beams emerge from the right surface of the AM-1 as shown in Fig. 3(b). For AM-2, we choose PT-2 acoustic beams as $y = -0.8x^{1/2}$ $(y \le 0)$ and $y = 0.8x^{1/2}$ $(y \ge 0)$. The corresponding spatial phase profile in the y-axis direction could be obtained as[28,29,31]

$$\phi(y) = 0.16k\left[\ln(\sqrt{y^2+0.0256}+y\right]. \quad (2)$$

In Fig. 4(a), the solid line shows the spatial phase profile in the y-axis direction based on Eq. (2) and the 80 scattered dots represent the transmitted phase shifts of 80 TAS subunits in the y-axis direction. Figure 4(b) shows the transmitted acoustic fields through AM-2. It is observed that PT-2 acoustic beams emerge from the right surface of the AM-2.

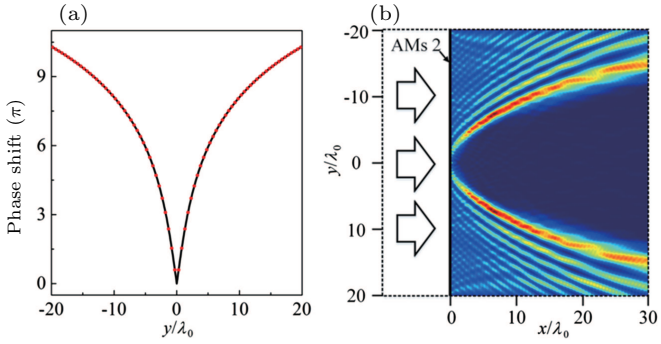


Fig. 4. (color online) (a) Spatial phase profile in y-axis direction for two parabolic trajectories [$y = -0.8x^{1/2}$ $(y \le 0)$ and $y = 0.8x^{1/2}$ $(y \ge 0)$] (PT-2) and (b) acoustic field distribution of PT-2 through AM-2. Scattered dots in panel (a) represent discrete phases of 80 subunits (one dot corresponds to one subunit).

3. Numerical results and discussion

Based on AM-1 and AM-2, we design the ATS to realize the controllable bidirectional asymmetric acoustic focusing. We define the distance from the center of ATS to the focus as the focal length. Figure 5(a) shows the simulated acoustic field distribution of the ATS for the PD case. Here, the working frequency is fixed at 3.432 kHz ($\lambda_0 = 10$ cm) and the space L between AM-1 and AM-2 is fixed at $8.5\lambda_0$. Perfectly matched layers (PMLs) are used around the model to prevent reflections. In this case, a focus with a short focal length of $\sim 6.82\lambda_0$ is found on the right of the ATS. To illustrate this acoustic focusing more clearly, we calculate the focal intensity contrast $|p/p_0|^2$ along and perpendicular to the x axis near the focal point [marked as dotted lines "I" and "II" in Fig. 5(a)], as shown in Figs. 5(b) and 5(c), respectively. Here, p and p_0 are the amplitude of the focused and incident wave, respectively. The full width at half maximum (FWHM) in Fig. 5(b) is about $0.42\lambda_0$ and in Fig. 5(c) is about $1.68\lambda_0$ and the maximal intensity contrast could reach about 34.6. Figure 5(d) shows the simulated acoustic field distribution of the same ATS for the ND case at the same working frequency of 3.432 kHz. Under this condition, a focus with a long focal length of $\sim 17.45\lambda_0$ is found on the left of the ATS. Figures 5(e) and 5(f) represent the intensity contrasts on lines I and II in Fig. 5(d), respectively. It is found that the FWHM is $\sim 0.38\lambda_0$ in Fig. 5(e) and $\sim 2.23\lambda_0$ in Fig. 5(f) and the maximum of $|p/p_0|^2$ value reaches about 30.9.

Figure 6 illustrates the intensity contrasts $|p/p_0|^2$ in dotted line "II" at working frequencies $f = 3.232$, 3.332, 3.432, 3.532, and 3.632 kHz, in which the structures of the ATSs are the same as those in Fig. 5. For the PD cases, the numerical simulation results reveal that the maximal $|p/p_0|^2$ values at $f = 3.232$, 3.332, 3.432, 3.532, and 3.632 kHz, are about 24.3, 36.3, 34.6, 27.2, and 17.2, respectively, as shown in Fig. 6(a). Meanwhile, the corresponding focal lengths are about $6.73\lambda_0$, $7.13\lambda_0$, $6.82\lambda_0$, $6.83\lambda_0$, and $6.81\lambda_0$, respectively and the corresponding FWHMs are $1.24\lambda_0$, $1.59\lambda_0$, $1.68\lambda_0$, $1.47\lambda_0$, and $1.58\lambda_0$, respectively. For the PD cases, the numerical simulation results reveal that the maximal $|p/p_0|^2$ values at $f = 3.232$, 3.332, 3.432, 3.532, and 3.632 kHz, are about 13.8, 25.7, 30.9, 30.8, and 24.5, respectively, as shown in Fig. 6(b). The focal lengths are about $15.85\lambda_0$, $16.65\lambda_0$, $17.45\lambda_0$, $18.12\lambda_0$, and $18.85\lambda_0$, respectively and the corresponding FWHMs are $2.15\lambda_0$, $2.26\lambda_0$, $2.23\lambda_0$, $1.85\lambda_0$, and $2.35\lambda_0$, respectively. It is obvious that the high focusing performances occur at these frequencies, which indicates that the working bandwidth of the BAAF based on our ATS could reach ~ 0.4 kHz.

We further study the influence of the space L between the AM-1 and AM-2 on the BAAF. Figures 7(a) and 7(b) show the acoustic field distributions of the ATS with $L = 12.5\lambda_0$ for the PD and ND case, respectively. Figures 7(c) and 7(d) show the acoustic field distribution of the ATS with $L = 16.5\lambda_0$ for the PD and ND case, respectively. The structures of two AMs are the same as those in Fig. 5 and the working frequency is 3.432 kHz. Compared with the results shown in Fig. 5, the intensity and focal length of the bidirectional asymmetric acoustic focusing are changed by adjusting the space L. The underlying mechanism could be intuitively understood as

the additional gradient phase profile change with the space L between AM-1 and AM-2.[28,29] To illustrate the change of asymmetric acoustic focusing more clearly, we calculate the focal length (dashed-circle line for the left-hand scale) and the corresponding intensity contrast $|p/p_0|^2$ (dashed-triangle line for the right-hand scale) of the ATSs as a function of L for the PD and ND case as shown in Figs. 7(e) and 7(f), respectively. For the PD case, it is observed that with increasing L value from $7.5\lambda_0$ to $17.5\lambda_0$ the focal length increases from $\sim 5.9\lambda_0$ and $\sim 11.5\lambda_0$, and the corresponding maximal $|p/p_0|^2$ value decreases rapidly from ~ 36 to ~ 1. For the ND case, with increasing L value, the focal length increases almost linearly from $\sim 16.5\lambda_0$ to $\sim 22.9\lambda_0$ while the corresponding maximal $|p/p_0|^2$ value decreases almost linearly from ~ 33 to ~ 20. It is found that, as $L = 17.5\lambda_0$, the focusing of the ATS in the PD case almost disappears while the focusing in the ND case still exists. In this case, a unidirectional acoustic focusing is achieved by our ATS. Therefore, without changing the structures of two AMs, the BAAF could be manipulated easily by mechanically adjusting the space L of two flat AMs.

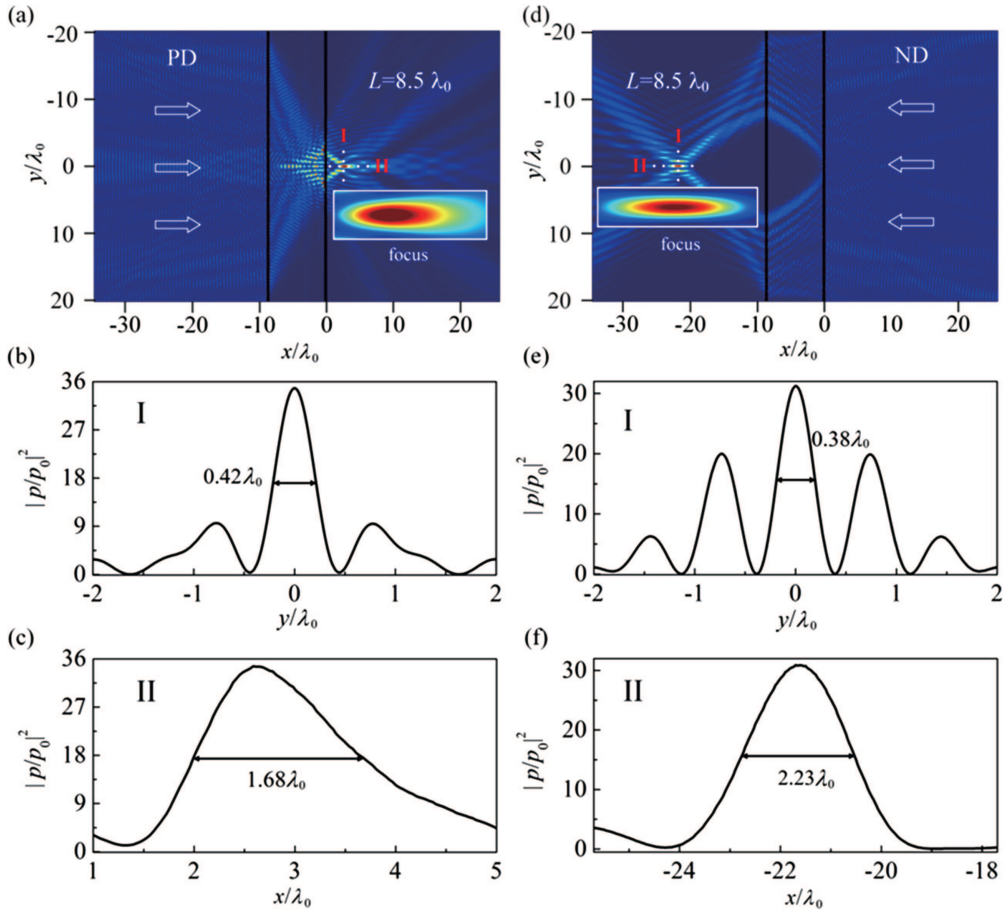


Fig. 5. (color online) (a) Acoustic field distribution of the ATS for PD case. (b) Intensity contrasts $|p/p_0|^2$ on dotted line "I" in panel (a). (c) Intensity contrast $|p/p_0|^2$ on dotted line "II" in panel (a)]. (d) Acoustic field distribution of the ATS for the ND case. (e) Intensity contrasts $|p/p_0|^2$ on dotted line "I" in panel (d). (f) Intensity contrasts $|p/p_0|^2$ on dotted line "II" in panel (d)]. The working frequency is fixed at 3.432 kHz and the space L between two AMs is fixed at $8.5\lambda_0$.

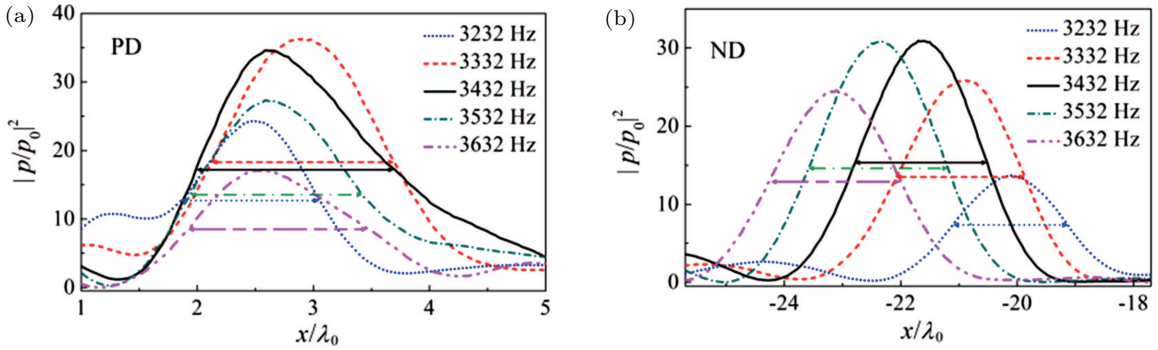


Fig. 6. (color online) Intensity contrasts $|p/p_0|^2$ on dotted line "II" for (a) PD case and (b) ND case at the working frequencies $f = 3.232$, 3.332, 3.432, 3.532, and 3.632 kHz, respectively. Structures of the ATSs are the same as those in Fig. 5.

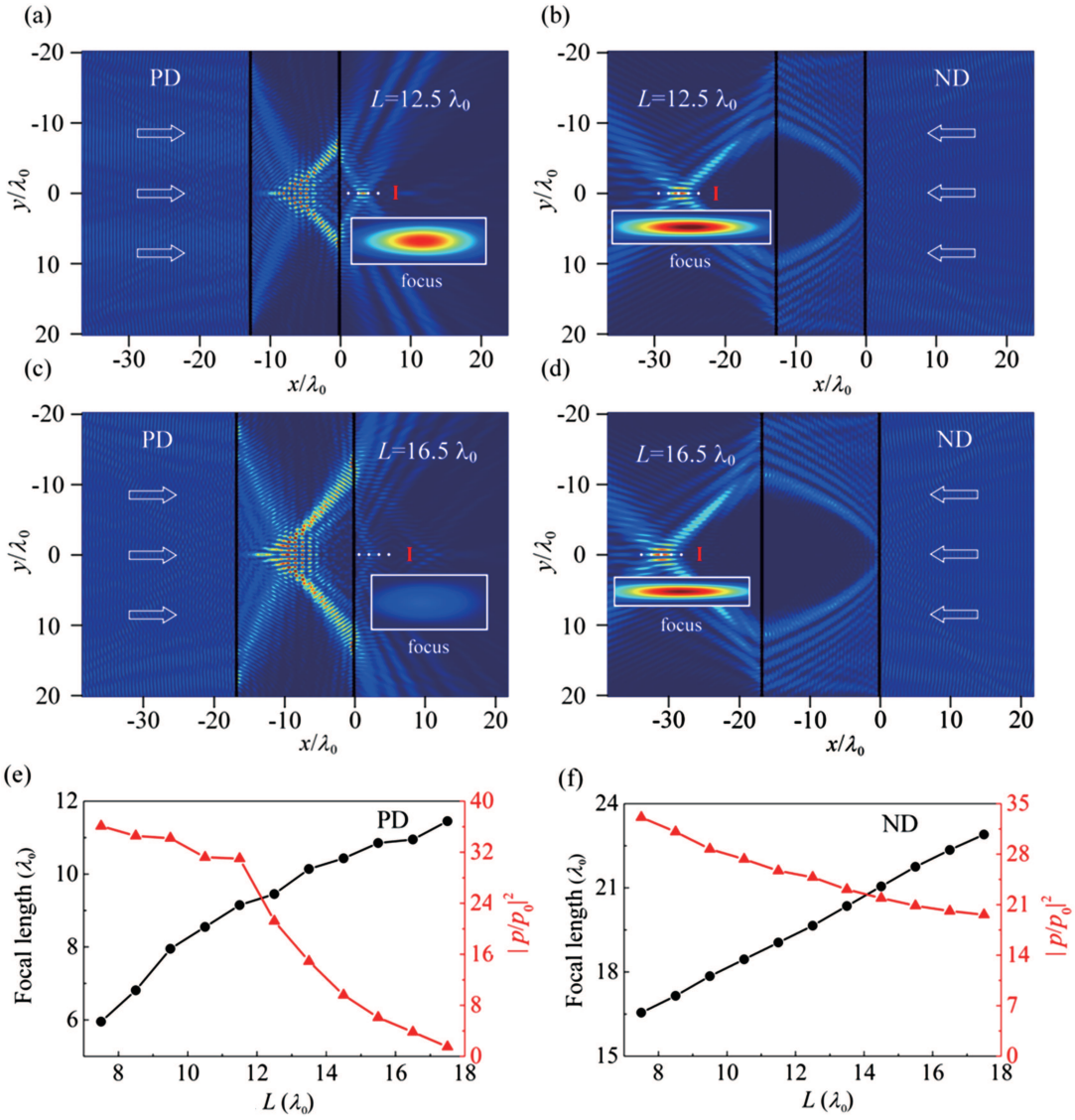


Fig. 7. (color online) Acoustic field distributions of acoustic plane waves impinging normally on ATS with $L = 12.5\lambda_0$ for (a) PD case and (b) ND case. Acoustic field distributions of the acoustic plane waves impinging normally on ATS with $L = 16.5\lambda_0$ for (c) PD case and (d) ND case. Focal length (dashed-circle line for the left-hand scale) and corresponding intensity contrast $|p/p_0|^2$ (dashed-triangle line for the right-hand scale) of the ATSs as a function of L for (e) PD case and (f) ND case. The working frequency is fixed at 3.432 kHz.

4. Conclusions

An ATS with two different flat AMs is proposed to achieve bidirectional asymmetric acoustic focusing. Two flat AMs with different phase profiles could generate different parabolic acoustic beams, which are used to realize the BAAF. Numerical simulations based on the FEM have been carried out to verify the proposed design. We have proven that the designed ATS for BAAF is robust within ~ 0.4 kHz frequency band. On the one side of the ATS, the acoustic wave is focused with a short focal length. Meanwhile, on the other side, the acoustic wave is focused with a long focal length. Moreover, we find that the intensities and focal lengths can be modulated by adjusting the space L between two flat AMs. Because the space L is larger than $\sim 17.5\lambda_0$, BAAF could be converted into unidirectional acoustic focusing. The proposed ATS with two AMs may provide more possibilities in controlling acoustic waves and it may find applications in focused ultrasound therapy and ultrasound imaging.

Acknowledgment

We thank those people or groups for their scientific contributions to this work.

References

[1] Zhu H F and Semperlotti F 2016 *Phys. Rev. Lett.* **117** 034302
[2] Xie Y B, Wang W Q, Chen H Y, Konneker A, Popa B I and Cummer S A 2014 *Nat. Commun.* **5** 5553
[3] Li Y, Jiang X, Li R Q, Liang B, Zou X Y, Yin L L and Cheng J C 2014 *Phys. Rev. Appl.* **2** 064002
[4] Mei J and Wu Y 2014 *New J. Phys.* **16** 123007
[5] Memoli G, Caleap M, Asakawa M, Sahoo D R, Drinkwater B W and Subramanian S 2017 *Nat. Commun.* **8** 14608
[6] Xie B Y, Tang K, Cheng H, Liu Z Y, Chen S Q and Tian J G 2017 *Adv. Mater.* **29** 1603507

[7] Xie B Y, Cheng H, Tang K, Liu Z Y, Chen S Q and Tian J G 2017 *Phys. Rev. Appl.* **7** 024010
[8] Li Y, Shen C, Xie Y B, Li J F, Wang W Q, Cummer S A and Jing Y 2017 *Phys. Rev. Lett.* **119** 035501
[9] Li Y, Liang B, Tao X, Zhu X F, Zou X Y and Cheng J C 2012 *Appl. Phys. Lett.* **101** 233508
[10] Yuan B G, Cheng Y and Liu X J 2015 *Appl. Phys. Express* **8** 027301
[11] Xie Y B, Shen C, Wang W Q, Li J F, Suo D J, Popa B I, Jing Y and Cummer S A 2016 *Sci. Rep.* **6** 35437
[12] Tang K, Qiu C Y, Ke M Z, Lu J Y, Ye Y T and Liu Z Y 2015 *Sci. Rep.* **4** 6517
[13] Zhu Y F, Zou X Y, Li R Q, Jiang X, Tu J, Liang B and Cheng J C 2015 *Sci. Rep.* **5** 10966
[14] Christensen J, RomeroGarcía V, Picó R, Cebrecos A, GarcíadeAbajo F J, Mortensen N A, Willatzen M and SánchezMorcillo V J 2015 *Sci. Rep.* **4** 4674
[15] Chen D C, Zhu X F, Wei Q, Wu D J and Liu X J 2018 *Appl. Phys. A* **124** 13
[16] Shen C, Xie Y B, Li J F, Cummer S A and Jing Y 2016 *Appl. Phys. Lett.* **108** 223502
[17] Jiang X, Liang B, Zou X Y, Yang J, Yin L L, Yang J, Cheng J C 2016 *Sci. Rep.* **6** 28023
[18] Liu B Y and Jiang Y Y 2018 *Appl. Phys. Lett.* **112** 173503
[19] Molerón M, Serra-Garcia M and Daraio C 2014 *Appl. Phys. Lett.* **105** 114109
[20] Climente A, Torrent D and SánchezDehesa J 2010 *Appl. Phys. Lett.* **97** 104103
[21] Zhao J J, Ye H P, Huang K, Chen Z N, Li B W and Qiu C W 2015 *Sci. Rep.* **4** 6257
[22] Zigoneanu L, Popa B I and Cummer S A 2011 *Phys. Rev. B* **84** 024305
[23] Cervera F, Sanchis L, SánchezPérez J V, MartínezSala R, Rubio C and Meseguer F 2001 *Phys. Rev. Lett.* **88** 023902
[24] Chen D C, Zhu X F, Wei Q, Wu D J and Liu X J 2018 *J. Appl. Phys.* **123** 044503
[25] Wang W Q, Xie Y B, Konneker A, Popa B I and Cummer S A 2014 *Appl. Phys. Lett.* **105** 101904
[26] Li Y, Qi S B and Assouar M B 2016 *New J. Phys.* **18** 043024
[27] Xia J P, Zhang X T, Sun H X, Yuan S Q, Qian J and Ge Y 2018 *Phys. Rev. Appl.* **10** 014016
[28] Epstein I and Arie A 2014 *Phys. Rev. Lett.* **112** 023903
[29] Greenfield E, Segev M, Walasik W and Raz O 2011 *Phys. Rev. Lett.* **106** 213902
[30] Tian Y, Wei Q, Cheng Y and Liu X J 2017 *Appl. Phys. Lett.* **110** 191901
[31] Chen D C, Zhu X F, Wei Q, Wu D J and Liu X J 2018 *Sci. Rep.* **8** 12682